ELSEVIER

Engineering Analysis with Boundary Elements 30 (2006) 49–58

ENGINEERING ANALYSIS *with* BOUNDARY ELEMENTS

www.elsevier.com/locate/enganabound

Effectiveness of GMRES-DR and OSP-ILUC for wave diffraction analysis of a very large floating structure (VLFS)

Noritoshi Makihata, Tomoaki Utsunomiya *, Eiichi Watanabe

Department of Civil and Earth Resources Engineering, Kyoto University, Kyoto 606-8501, Japan

Received 12 November 2004; revised 10 May 2005; accepted 19 August 2005
Available online 19 October 2005

Abstract

This paper presents the performance of iterative solvers and preconditioners for the non-Hermitian dense linear systems arising from the boundary value problem related to the diffraction wave field around a very large floating structure (VLFS). These systems can be solved iteratively using the GMRES with deflated restarting (GMRES-DR), which has Krylov subspaces with approximate eigenvectors as starting vectors. The number of iteration needed by GMRES or GMRES-DR can be significantly reduced using preconditioning techniques. Matrix-vector products are approximated by utilizing the fast multipole method (FMM), which need not directly calculate the dense matrix of the far field interactions. The combination of the operator splitting preconditioner (OSP) and the Crout version of the incomplete LU factorization (ILUC) does not require the dense matrix of the far field interactions. Numerical experiments from a hybrid-type VLFS, which is composed of pontoon-part and semi-submersible part, whose length is 3000 m are presented.

Keywords: Iterative methods; GMRES; Boundary element method; Preconditioning; Operator splitting; Incomplete LU factorization; Fast multipole method; VLFS

1. Introduction

The problem of the interaction between the global structural response of a very large floating structure (VLFS) and the associated diffraction wave field in an unbounded exterior domain is achieved here by matching a boundary element analysis of the exterior diffraction wave field with a finite element analysis of the elastic structure at the fluid-structure interface. We finally arrive at solving a large system of linear equations of the form

$$Ax = b, \tag{1}$$

where the coefficient matrix A is non-Hermitian and dense (see Refs. [1,2]).

The generalized minimal residual method (GMRES) [3] is a well-known iterative method for solving large non-Hermitian linear systems of equations. Since GMRES becomes increasingly expensive and requires more storage as the iteration proceeds, it generally uses restarting, which slows the convergence. The GMRES with deflated restarting (GMRES-DR) [4] is derived from restarting implicitly with an appropriate vector, which is a linear combination of the approximate eigenvectors obtained from the orthogonal projection method [5] onto Krylov subspaces [3–5]. The deflation of eigenvalues can greatly improve the convergence rate of restarted GMRES.

It is well known that the convergence rate of Krylov subspace methods for linear equations depends on the spectrum of A [6]. It is therefore natural to try to transform the original system (1) into one having the same solution but more favorable spectral properties. A preconditioner is a matrix that can be used to accomplish such a transformation. The operator splitting preconditioner (OSP) [7,8] is an effective technique in solving dense linear systems arising from the boundary element method (BEM). OSP splits the coefficient matrix A into the sparse matrix A_{near} of the near field interactions and the dense matrix A_{far} of the far field interactions. Out of A_{near}, the preconditioner M is constructed using the Crout version of the incomplete LU factorization (ILUC) [9]. Matrix-vector products are approximated by utilizing the fast multipole method (FMM) [10,11], which need not directly calculate A_{far}. The OSP-ILUC preconditioner does not require A_{far}. Therefore, it can be expected that the boundary element method using FMM will be further accelerated by OSP-ILUC.

In the first part of this paper, we apply GMRES-DR to the analysis of the boundary value problem related to

* Corresponding author. Tel.: +81 75 753 5078; fax: +81 75 753 5130.
E-mail address: utsunomi@str.kuciv.kyoto-u.ac.jp (T. Utsunomiya).

0955-7997/$ - see front matter © 2005 Elsevier Ltd. All rights reserved.
doi:10.1016/j.enganabound.2005.08.006

the diffraction wave field around a very large floating structure (VLFS).

In the second part, we apply OSP-ILUC to our example. OSP has a parameter r, which is the minimum distance of far points. We show that OSP becomes ineffective if r is too large. We clarify the range of r where OSP is effective at the same time.

2. Integral equation formulation

Example that is investigated is shown in Fig. 1, which is a hybrid-type VLFS, which is composed of pontoon-part and semi-submersible part, floating in the open sea with constant depth h, whose length is L, whose width is B, and whose draft is d [1]. The coordinate system is defined such that the xy plane locates on the undisturbed free surface and the z-axis points upward. The longcrested harmonic wave with small amplitude is considered. The amplitude of the incident wave is defined by A, the circular frequency by ω, and the angle of incidence by β. $\beta=0$ corresponds to the head wave from positive x direction and $\beta=\pi/2$ to the beam wave from positive y direction.

Assuming the water to be perfect fluid with no viscosity and incompressible, and the fluid motion to be irrotational, then the fluid motion can be represented by a velocity potential Φ. Also, we consider the steady-state harmonic motions of the fluid and the structure, with the circular frequency ω. Then, all of the time-dependent quantities can be represented similarly as follows:

$$\Phi(x,y,z,t) = \mathrm{Re}[\phi(x,y,z)\mathrm{e}^{\mathrm{i}\omega t}], \tag{2}$$

where i is the imaginary unit and t is the time.

Assuming the fluid motion to be small, we can employ the linearized wave theory. Then, our problem is formulated as the boundary value problem represented by a velocity potential ϕ as follows:

$$\nabla^2\phi = 0 \quad \text{in } \Omega \tag{3}$$

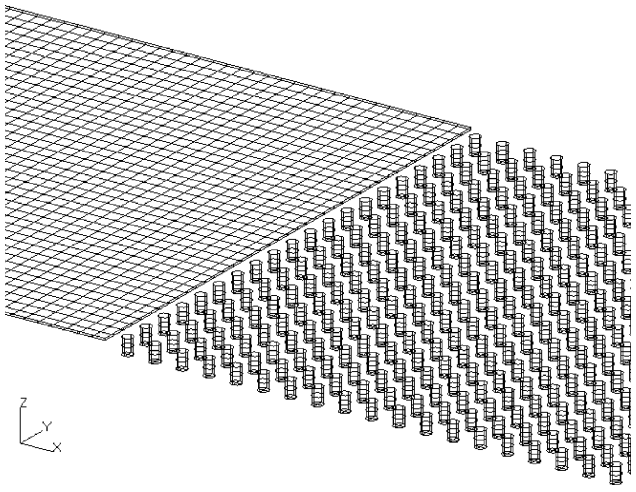

Fig. 1. A hybrid-type VLFS [1].

$$\frac{\partial\phi}{\partial z} = K\phi \quad \text{on } S_{\mathrm{F}} \tag{4}$$

$$\frac{\partial\phi}{\partial z} = 0 \quad \text{on } B_0 \tag{5}$$

$$\frac{\partial\phi}{\partial n} = 0 \quad \text{on } S_{\mathrm{H}} \tag{6}$$

$$\lim_{r\to\infty}\sqrt{r}\left(\frac{\partial(\phi-\phi_I)}{\partial r} - \mathrm{i}k(\phi-\phi_{\mathrm{I}})\right) = 0 \quad \text{on } S_\infty \tag{7}$$

$$\phi_{\mathrm{I}} = \mathrm{i}\frac{gA}{\omega}\frac{\cosh k(z+h)}{\cosh kh}\mathrm{e}^{\mathrm{i}k(x\cos\beta + y\sin\beta)} \tag{8}$$

Here, ϕ_{I} is the incident wave potential. The fluid domain is defined by the symbol Ω, the undisturbed free surface by S_{F}, the flat bottom base surface of $z=-h$ by B_0, the wetted-surface of VLFS by S_{H}, and the boundary at infinity by S_∞. The symbol n represents the normal vector (positive direction is out of fluid domain into the body inner part), and r is a horizontal distance from the origin. The symbol K is the wave number in the infinite depth ($=\omega^2/g$; g is the gravitational acceleration), and k is the wave number. Then, the following dispersion relation is satisfied:

$$k\tanh kh = K \tag{9}$$

Substituting the boundary conditions represented by a velocity potential ϕ into the integral equation, we have the following integral equation [12]:

$$4\pi\phi(x) + \int_{S_{\mathrm{H}}}\left\{\phi(\xi)\frac{\partial G(x,\xi)}{\partial n_\xi} - \phi(x)\frac{\partial G_2(x,\xi)}{\partial n_\xi}\right\}\mathrm{d}\xi = 4\pi\phi_{\mathrm{I}}(x) \tag{10}$$

Here, $G(x,\xi)$ is called the free-surface Green's function and it is a fundamental solution of the Laplacian ∇^2 which satisfies boundary conditions (4), (5) and (7), and $G_2(x,\xi)$ is the auxiliary Green's function which corresponds to a rigid free surface condition [12]. From the integral Eq. (10) we arrive at a system of linear equations, whose solution is the potentials at nodes after discretization of the S_{H} surface [1,11].

3. GMRES with deflated restarting

It is well known that the convergence rate of GMRES for linear equations depends on the distribution of eigenvalues of the coefficient matrix A. Therefore, deflating small eigenvalues can greatly improve the convergence rate. The GMRES with deflated restarting (GMRES-DR) [4] is derived from restarting implicitly with an appropriate vector, which is a linear combination of harmonic Ritz vectors [4].

3.1. Harmonic Ritz pairs

Definition 1. Let A be an $n\times n$ complex matrix and T be an m dimensional subspace of $\mathbf{C}^n$. A pair (θ,y), where θ is a complex number and y is a non-zero vector in T, is called a Ritz pair

of A in T if the following Galerkin condition is satisfied: $Ay-\theta y \perp T$.

We let m be the maximum dimension of the subspace. Also, we let x_0 be an initial guess for the solution of a linear system (1) and define the initial residual $r_0=b-Ax_0$. We define $K_m(A,r_0)=\mathrm{Span}\{r_0, Ar_0,\ldots, A^{m-1}r_0\}$ the mth Krylov subspace generated by the matrix A and the vector r_0. We let r_m be the mth GMRES residual. Also, we let V_{m+1} be the $n\times(m+1)$ complex matrix and $\bar{H}_m$ be the $(m+1)\times m$ complex matrix from the Arnoldi recurrence [5]: $AV_m=V_mH_m+h_{m+1,m}v_{m+1}e_m^H=V_{m+1}\bar{H}_m$. Note that V_m denotes an $n\times m$ matrix and H_m denotes an $m\times m$ matrix. By V_{m+1}^H and e_m^H, we denote the Hermitian transpose of V_{m+1} and the mth unit vector e_m, respectively.

Definition 2. A pair (θ,y) is called a harmonic Ritz pair if (θ,y) is a Ritz pair of A in $AK_m(A,r_0)$.

Proposition 3. Define

$$\bar{c}=\begin{bmatrix} c \\ c_{m+1}\end{bmatrix}:=V_{m+1}^H r_m \quad \text{and } G_m:=H_m-\frac{h_{m+1,m}}{c_{m+1}}ce_m^H.$$

Let (θ,g) be an eigenpair of G_m and define $y=V_mg$, then (θ, y) is a harmonic Ritz pair.

3.2. Keeping the subspace a Krylov subspace

The first cycle of GMRES-DR is standard GMRES with r_0 being the residual vector computed. At the end of the cycle, $r_0=r_m$ and the l desired harmonic Ritz vectors $y_1,\ldots,y_l$ are computed. Then the subspace S generated by the second cycle is

$$S=\mathrm{Span}\{y_1,\ldots,y_l,r_0,Ar_0,\ldots,A^{m-l-1}r_0\}. \tag{11}$$

It can be shown that GMRES-DR keeps the generated subspace S a Krylov subspace, i.e.

$$S=K_m(A,s), \tag{12}$$

where s is a linear combination of $y_1,\ldots,y_l$ (see Ref. [4]).

3.3. The algorithm of GMRES-DR

The algorithm of GMRES-DR is sketched next. We assume that the harmonic Ritz values, which are eigenvalues of G_m are distinct.

3.3.1. GMRES-DR

(1) Choose m, the maximum size of the subspace, and l, the desired number of harmonic Ritz vectors. Choose an initial guess x_0 and compute $r_0=b-Ax_0$. Let $v_1=r_0/\|r_0\|_2$ and $\bar{c}=\|r_0\|_2e_1$.
(2) Generate V_{m+1} and $\bar{H}_m$ with the Arnoldi iteration.
(3) Solve min $\|\bar{c}-\bar{H}_md\|_2$ for d. Let $x_0=x_0+V_md$, $\bar{c}=\bar{c}-\bar{H}_md$.
(4) Let $G_m=H_m-\frac{h_{m+1}}{c_{m+1}}ce_m^H$. Then compute the l smallest eigenpairs $\{(\theta_i,g_i)|i=1,\ldots,l\}$ of G_m.
(5) Orthonormalize $g_1,\ldots,g_l$ to form an $m\times l$ matrix Q_l. Extend $q_1,\ldots,q_l$ to length $m+1$ by appending a zero entry to each. Then orthonormalize $\bar{c}$ against them to form q_{l+1}. Let $\bar{c}=Q_{l+1}^H\bar{c}$, $\bar{H}_l^{\mathrm{new}}=Q_{l+1}^H\bar{H}_mQ_l$ and $V_{l+1}^{\mathrm{new}}=V_{m+1}Q_{l+1}$. Then let $\bar{H}_l=\bar{H}_l^{\mathrm{new}}$ and $V_{l+1}=V_{l+1}^{\mathrm{new}}$.
(6) Extend V_{l+1} and $\bar{H}_l$ to V_{m+1} and $\bar{H}_m$ by the Arnoldi iteration. Go to (3).

4. Numerical experiments without preconditioning

Example that is investigated is the hybrid-type VLFS (See Fig. 1) floating in the open sea, whose main specifications are shown in Table 1. The wave diffraction analysis has been made for the oblique incident wave ($\beta=\pi/3$) whose wavelengths are $\lambda=121.21$ m or $\lambda=88.77$ m.

The eight-noded quadrilateral panel element is used. The pontoon-part is discretized by 10 m×10 m panels for the bottom surface and 10 m×1.5 m panels for the side surfaces. The number of elements is 8480 and the number of nodes is 25, 921 for pontoon-part, the number of elements is 12,000 and the number of nodes is 44,000 for semisub-part, and the number of elements is 20,480 and the number of nodes is 69,921 for hybrid-type VLFS. GMRES-DR, restarted GMRES, unrestarted full GMRES and GPBi-CG [13] were used to solve the linear systems using a zero initial guess. The experiments were conducted using double-precision arithmetic on IBM RS/6000SP (CPU POWER3 375 MHz; one node).

Performances of GMRES-DR and restarted GMRES for pontoon-part are shown in Tables 2 and 3. Also, performances of GMRES-DR and restarted GMRES for hybrid-type VLFS are shown in Table 4. The symbol m is a parameter of GMRES-DR or restated GMRES, which is the maximum dimension of the subspace. The symbol l is a parameter of GMRES-DR, which is the number of approximate eigenvectors retained at a restart. 'Its' denotes the number of iterations for GMRES-DR or restarted GMRES. 'It(s)' denotes the iteration time in seconds. The iterations were terminated when the residual norm was reduced by five orders of magnitude. Two parameters m and l are chosen in a way that the total amount of memory required by GMRES-DR is the same as that by restarted GMRES.

Figs. 2 and 3 show residual norms plotted against the number of iterations for pontoon-part. Unrestarted full GMRES

Table 1
Main specifications of the VLFS [1]

Type of VLFS	Pontoon	Semisub	Hybrid
Deck length (m)	2000	1000	3000
Deck width (m)	400	400	400
Draft (m)	1.5	12.0	1.5&12.0
Diameter of columns (m)	–	8.0	8.0
Number of columns	–	1000	1000
Spacing between columns (m)	–	20.0	20.0
Water depth (m)	20.0	20.0	20.0

Table 2
Performances of GMRES-DR and restarted GMRES for a wavelength at 121.21 m, as l varies. $n=25921$, $m=100$.

	GMRES-DR(m,l)		GMRES($m+l$)	
l	Its	It(s)	Its	It(s)
10	833	24596.0	1164	33430.0
20	836	24699.0	1150	34035.9
30	849	25121.6	1097	33856.2

reaches the required residual with 340 iterations for a wavelength at 121.21 m and with 614 iterations at 88.77 m, but it requires about three times more storage than the restarted GMRES. GPBi-CG reaches the required residual with 1286 iterations for a wavelength at 121.21 m and with 3044 iterations at 88.77 m. GPBi-CG requires about 10 times less storage or about 20 times less storage than GMRES-DR for respective wave lengths, but it is inferior to restarted GMRES if we have sufficient memory for the restarted GMRES.

Comparison of convergence for hybrid-type VLFS is shown in Fig. 4. Unrestarted full GMRES reaches the required residual with 426 iterations for a wavelength at 121.21 m, but it requires about four times more storage than the restarted GMRES. GPBi-CG does not reach the required residual within 4000 iterations. Therefore, we may think that the GMRES-DR solver performs best in these environments if the total amount of memory is restricted. These figures also show that the number of iterations needed by GMRES-DR can be significantly reduced as it is compared with restarted GMRES, when l is chosen to be $l/m=1/10$ regardless of incident wavelengths λ for our example. In each cycle, GMRES-DR stores the l dimensional subspace generated by the desired harmonic Ritz vectors, and extends it to the new subspace of dimension m by $m-l$ step. Therefore, these m dimensional subspaces will stagnate if l is chosen to be large.

5. Construction of the preconditioner

The number of iterations needed by GMRES may be significantly reduced using preconditioning techniques.

Let M be a preconditioner. We transform the original system (1) into

$$AM^{-1}y = b; \quad x = M^{-1}y. \tag{13}$$

As is known, there are two somewhat self-conflicting requirements of the preconditioner. The first one is efficiency, that is, the extra work required to solve $Mx=y$ should be easier than solving original system (1). Practically this means that M must be sparse or a product of sparse matrices. The second requirement is that the preconditioned matrix AM^{-1} should have clustered eigenvalues. Then it can be expected that the number of iterations needed by GMRES can be reduced according to the following inequality

$$\frac{||r_m||_2}{||r_0||_2} \le \frac{L}{2\pi\varepsilon} \inf_{\substack{p_m \in P_m \\ p_m(0)=1}} ||p_m||_{\Lambda_\varepsilon}. \tag{14}$$

Here, ε is a positive real number, Λ_ε is the ε-pseudospectrum of AM^{-1}, L is the arc length of the boundary (Λ_ε, P_m is the set of all polynomials of degree m and r_m is the residual of x_m (see Ref. [6]).

Table 3
Performances of GMRES-DR and restarted GMRES for a wavelength at 88.77 m, as l varies. $n=25921$, $m=200$

	GMRES-DR(m,l)		GMRES($m+l$)	
l	Its	It(s)	Its	It(s)
20	1578	46554.7	2353	68482.1
40	1598	46791.3	2272	66389.9
60	1638	48114.4	2217	64536.5

Table 4
Performances of GMRES-DR and restarted GMRES for a wavelength at 121.21 m, as l varies. $n=69921$, $m=100$.

	GMRES-DR(m,l)		GMRES($m+l$)	
l	Its	It(s)	Its	It(s)
10	1694	178478.0	2576	269379.9
20	1487	156799.9	2512	263518.2
30	1410	148922.9	2432	254808.8

5.1. Operator splitting preconditioners

For any $x \in S_H$

$$\lim_{\xi \to x} |G(x,\xi)| = +\infty, \tag{15}$$

where $G(x,\xi)$ is the free-surface Green's function, so the absolute value of the corresponding entry a_{ij} of A is large if a node x_j is near the node x_i for any node x_i.

If r is a positive real number, the matrix $A_{\text{near}}(r)$ of the near field interactions of A and the matrix $A_{\text{far}}(r)$ of the far field interactions of A are defined by

$$A_{\text{near}}(r)_{ij} = \begin{cases} a_{ij} & \text{if } ||x_i - x_j||_2 \le r, \\ 0 & \text{otherwise,} \end{cases} \tag{16}$$

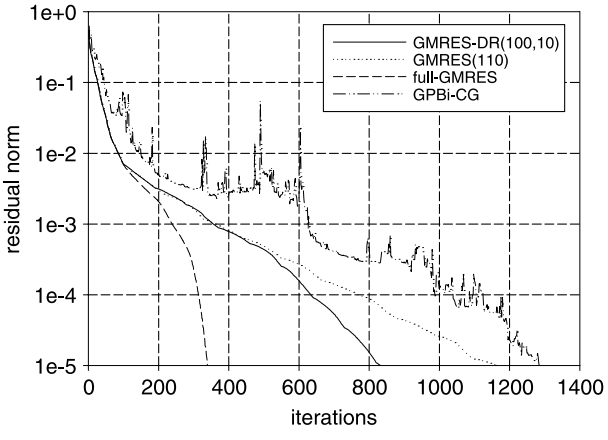

Fig. 2. Comparison of convergence for a wavelength at 121.21 m. $n=25921$.

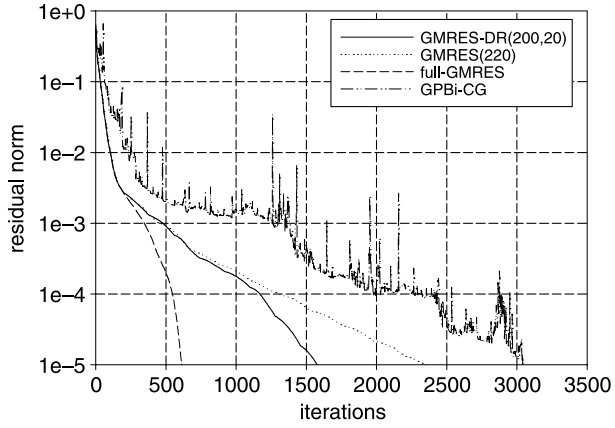

Fig. 3. Comparison of convergence for a wavelength at 88.77 m. $n=25921$.

$$A_{\text{far}}(r)_{ij} = \begin{cases} a_{ij} & \text{if } ||x_i - x_j||_2 > r, \\ 0 & \text{otherwise.} \end{cases} \tag{17}$$

Then A is split as follows:

$$A = A_{\text{near}}(r) + A_{\text{far}}(r). \tag{18}$$

If M approximates $A_{\text{near}}(r)$,

$$AM^{-1} \approx \{A_{\text{near}}(r) + A_{\text{far}}(r)\}A_{\text{near}}(r)^{-1} \tag{19}$$

$$= I + A_{\text{far}}(r)A_{\text{near}}(r)^{-1} \tag{20}$$

Therefore, if r can be chosen so that $\|A_{\text{far}}(r)A_{\text{near}}(r)^{-1}\|_2$ is small, it can be expected that all eigenvalues of AM^{-1} will cluster around 1. Moreover we require that r be chosen so that $A_{\text{near}}(r)$ is computed directly in FMM [10,11] and it is sparse. These preconditioners are called the operator splitting preconditioners (OSP) [7].

5.2. Crout version of ILU

Among the most popular preconditioners are those based on incomplete factorizations obtained from the LU factorization. Herein, a preconditioner M is constructed out of $A_{\text{near}}(r)$ using the Crout version of the incomplete LU factorization (ILUC) [9].

The algorithm of ILUC is sketched next. To avoid breakdown, we increased the diagonal element to 10^{-3} whenever some diagonal element in any of our algorithms to compute a preconditioner was found to be small, in our case less in absolute value than the IEEE machine precision $\varepsilon \approx 2.2 \cdot 10^{-16}$. *Applying the dropping rule* means 'selecting the p largest elements by utilizing a heap-sort strategy'.

5.2.1. ILUC

do $k=1,\ldots,n$
 do $j=k,\ldots,n$
  $z_j = a_{kj}$
 end do
 do $i=1,\ldots,k-1$; $l_{ki} \neq 0$
  do $j=k,\ldots,n$; $u_{ij} \neq 0$
   $z_j = z_j - l_{ki}u_{ij}$
  end do
 end do
 do $j=k+1,\ldots,n$
  $w_j = a_{jk}$
 end do
 do $i=1,\ldots,k-1$; $u_{ik} \neq 0$
  do $j=k+1,\ldots,n$; $l_{ji} \neq 0$
   $w_j = w_j - l_{ji}u_{ik}$
  end do
 end do
  if ($|z_k| <$ eps) then
 $z_k = 10^{-3}$
 end if
 $d_k = z_k$
 Apply the dropping rule to $z_{k+1:n}$
 do $j=k+1,\ldots,n$
  if ($|z_j| \geq \tau$) then
   $u_{kj} = z_j$
  end if
 end do

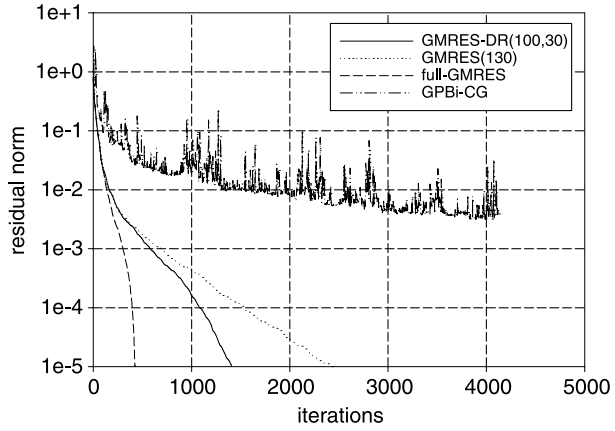

Fig. 4. Comparison of convergence for a wavelength at 121.21 m. $n=69921$.

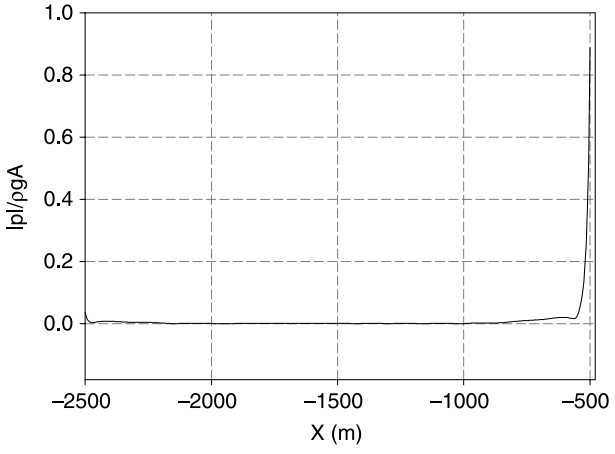

Fig. 5. Pressure on the bottom surface along centerline of pontoon-part for a wavelength at 88.77 m.

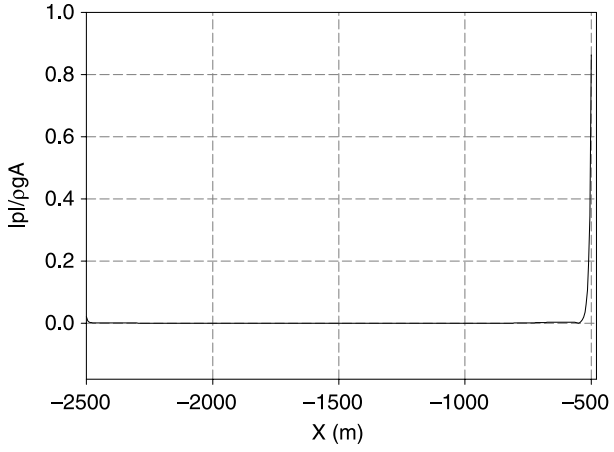

Fig. 6. Pressure on the bottom surface along centerline of pontoon-part for a wavelength at 55.03 m.

Apply the dropping rule to $w_{k+1:n}$
do $j=k+1,\ldots,n$
if ($|w_j| \geq \tau$) then
$l_{jk} = w_j/d_k$
end if
end do
end do

ILUC is controlled by two parameters τ and p. With the parameter τ, the minimal size of an entry in the factors L and U is prescribed. The second parameter p controls the maximum number of fill-in elements of L per column and of U per row.

6. Numerical experiments with preconditioning

Example that is investigated is the hybrid-type VLFS (See Fig. 1) floating in the open sea, whose main specifications are shown in Table 1. The wave diffraction analysis has been made for the oblique incident wave ($\beta=\pi/3$) whose wavelengths are $\lambda=88.77$ m or $\lambda=55.03$ m. Also, we have compared the spectrum of the coefficient matrix AM^{-1} transformed by OSP-ILUC with that of A without preconditioning.

The eight-noded quadrilateral panel element is used. The pontoon-part is discretized by 10 m×10 m panels for the bottom surface and 10 m×1.5 m panels for the side surfaces. The number of elements is 8480 and the number of nodes is 25, 921 for pontoon-part, the number of elements is 12,000 and the number of nodes is 44,000 for semisub-part, and the number of elements is 20,480 and the number of nodes is 69,921 for hybrid-type VLFS. GMRES was used to solve the linear systems using a zero initial guess. Matrix-vector products are approximated by utilizing the fast multipole method (FMM) [10,11]. The experiments were conducted using double-precision arithmetic with thread parallel computing (32CPU) on a FUJITSU PRIMEPOWER HPC2500 in Academic Center for Computing and Media Studies, Kyoto University. We chose the approximate eigenvalues as the harmonic Ritz values [4].

Pressures on the bottom surface along centerline of pontoon-part for wavelengths at $\lambda=88.77$ m and at $\lambda=55.03$ m are shown in Figs. 5 and 6, respectively.

Performances of OSP-ILUC for wavelengths at 88.77 m and at 55.03 m are shown in Tables 5 and 6, respectively. For two parameters τ and p on ILUC(τ,p), we use $\tau=10^{-5}$ and $p=0.025\times n$. r is a parameter of OSP, which is the minimum distance of far points. $r=0$ means that the preconditioner is not applied. 'Ratio$_A$' denotes the value of (the number of non-zero elements of $A_{\text{near}}(r)$)/(the number of non-zero elements of A). 'Ratio$_M$' denotes the value of (the number of non-zero elements in the ILUC of M)/(the number of nonzero elements of A), whose upper limit is $2p/n(=0.05)$. 'Its' denotes the number of iterations for GMRES, 'Pre(s)' denotes the time in seconds to build the preconditioners, 'It(s)' denotes the iteration time in seconds and 'Tot(s)' denotes the total time in seconds. The iterations were stopped when the residual norm

Table 5
Performance of OSP-ILUC for a wavelength at 88.77 m, as r varies

r(m)	Ratio$_A$	Ratio$_M$	Its	Pre(s)	It(s)	Tot(s)
Pontoon-part (n=25,921)						
0	0.000	0.000	407	0	3755	3755
20	0.002	0.007	295	121	2735	2856
40	0.007	0.031	192	316	1913	2229
60	0.014	0.048	164	435	1583	2018
80	0.024	0.049	189	379	1793	2172
Semisub-part (n=44,000)						
0	0.000	0.000	24	0	492	492
20	0.003	0.008	13	445	269	714
40	0.011	0.038	19	1359	415	1774
60	0.026	0.048	16	1741	362	2103
80	0.044	0.049	16	2011	358	2369
Hybrid-type VLFS (n=69,921)						
0	0.000	0.000	680	0	21562	21562
20	0.001	0.004	313	959	10020	10979
40	0.005	0.020	192	2856	7827	10683
60	0.012	0.041	166	3836	5502	9338
80	0.021	0.048	186	4233	6368	10601

Table 6
Performance of OSP-ILUC for a wavelength at 55.03 m, as r varies

r(m)	Ratio$_A$	Ratio$_M$	Its	Pre(s)	It(s)	Tot(s)
Pontoon-part (n=25,921)						
0	0.000	0.000	649	0	7404	7404
20	0.002	0.008	320	136	3031	3167
40	0.007	0.041	221	291	2246	2537
60	0.014	0.049	393	367	3908	4275
Semisub-part (n=44,000)						
0	0.000	0.000	103	0	2111	2111
20	0.003	0.008	54	357	1125	1482
40	0.011	0.042	60	1157	1304	2461
60	0.026	0.049	150	1441	3354	4795
Hybrid-type VLFS (n=69,921)						
0	0.000	0.000	1879	0	64363	64363
20	0.001	0.005	623	932	20007	20939
40	0.005	0.025	310	2125	10198	12323
60	0.012	0.048	578	5714	21171	26885

was reduced by five orders of magnitude. The number of iterations for GMRES increases if r is chosen to be 80 m in Table 5 or if r is chosen to be 60 m in Table 6. It is found that r cannot be chosen to be large. With application of OSP-ILUC we have succeeded in reducing the total computing times by 1/2 as compared without application of a preconditioner for our example. In Table 6 it is found that the total computing time is reduced by 1/5 for hybrid-type VLFS.

Spectra of pontoon-part for various r are shown in Figs. 7–10. It is found that the spectrum of AM^{-1} clusters as r increases. Comparisons of the spectrum for semisub-part without application of a preconditioner and with application of OSP-ILUC are shown in Figs. 11 and 12. It is found that the spectrum of A which is the coefficient matrix without application of a preconditioner has already clustered. Comparisons of the spectrum for hybrid-type VLFS without application of a preconditioner and with application of OSP-ILUC are shown in Figs. 13 and 14. The spectrum for hybrid-type VLFS is the union of the spectrum for pontoon-part

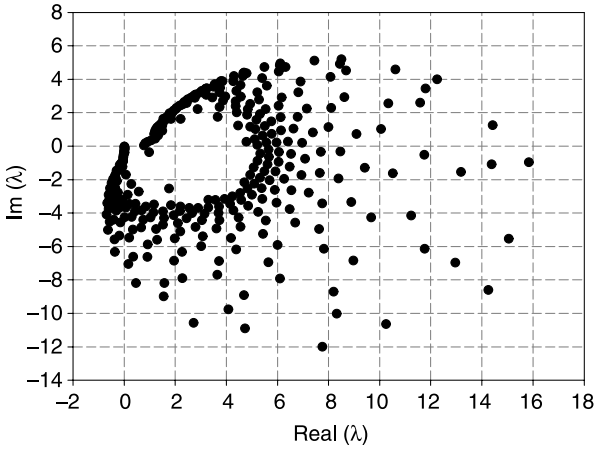

Fig. 8. Spectrum of pontoon-part for a wavelength at 55.03 m. n=25921. r=20 m. Its=320. Tot=3167.

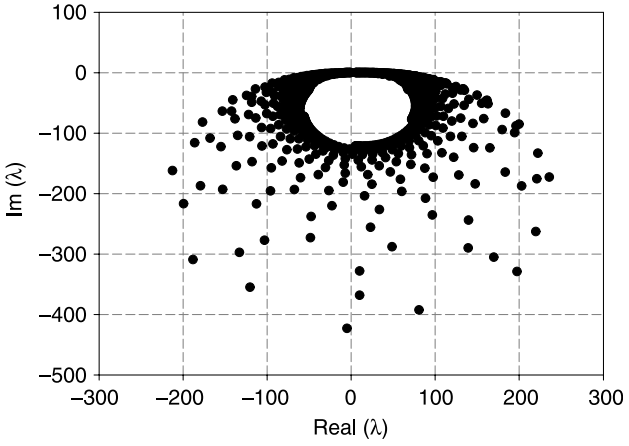

Fig. 7. Spectrum of pontoon-part for a wavelength at 55.03 m. n=25921. r=0 m. Its=649. Tot=7404.

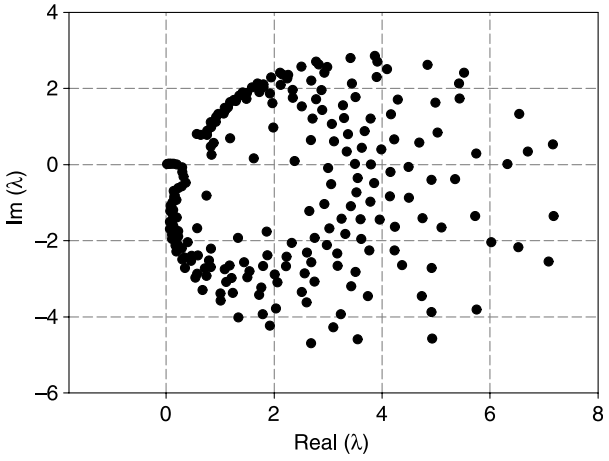

Fig. 9. Spectrum of pontoon-part for a wavelength at 55.03 m. n=25921. r=40 m. Its=221. Tot=2537.

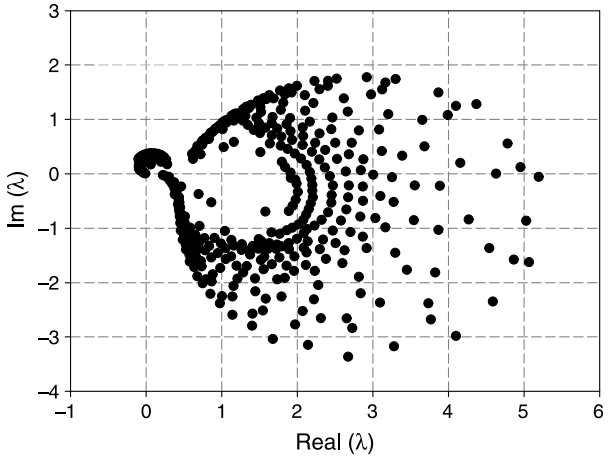

Fig. 10. Spectrum of pontoon-part for a wavelength at 55.03 m. $n=25921$. $r=60$ m. Its=393. Tot=4275.

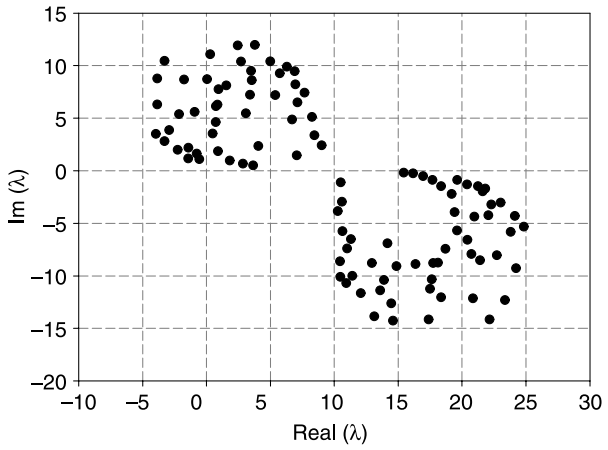

Fig. 11. Spectrum of semisub-part for a wavelength at 55.03 m. $n=44000$. $r=0$ m. Its=103. Tot=2111.

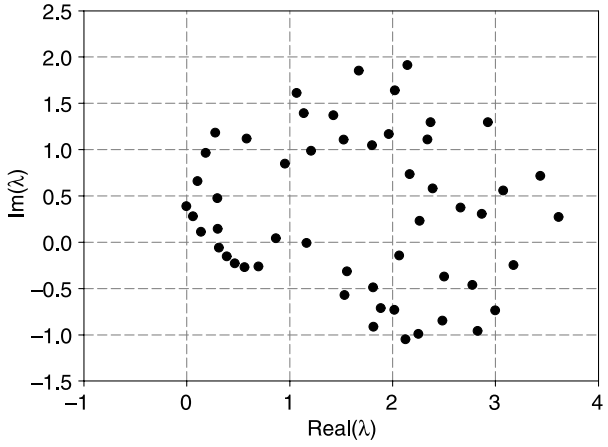

Fig. 12. Spectrum of semisub-part for a wavelength at 55.03 m. $n=44000$. $r=20$ m. Its=54. Tot=1482.

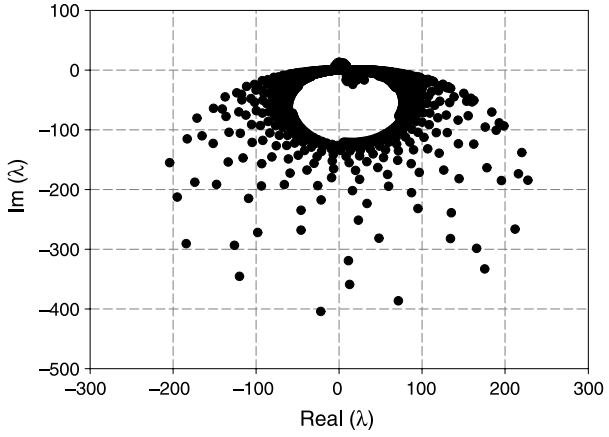

Fig. 13. Spectrum of hybrid-type VLFS for a wavelength at 55.03 m. $n=69921$. $r=0$ m. Its=1879. Tot=64363.

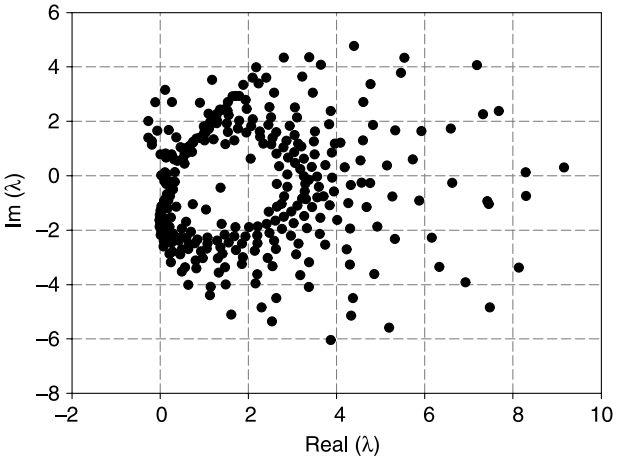

Fig. 14. Spectrum of hybrid-type VLFS for a wavelength at 55.03 m. $n=69921$. $r=40$ m. Its=310. Tot=12323.

Table 7
Number of iterations for GMRES using OSP-ILUC to converge for various r/λ

r/λ	$\lambda=55.03$ m	$\lambda=88.77$ m	$\lambda=121.21$ m	$\lambda=152.33$ m
Pontoon-part ($n=25{,}921$)				
0.0	649	407	277	205
0.2	557	317	215	159
0.4	284	204	146	111
0.6	227	166	120	94
0.7	224	165	121	93
0.8	226	174	127	97
1.0	335	228	156	105
1.2	–	245	138	79
Hybrid-type VLFS ($n=69921$)				
0.0	1879	680	384	254
0.2	1328	385	251	182
0.4	580	235	162	110
0.6	349	165	117	90
0.7	314	169	125	91
0.8	327	170	126	94
1.0	392	222	140	95
1.2	672	239	138	89

and that for semisub-part. It is found that the spectrum of AM^{-1} clusters.

Numbers of iterations for GMRES using OSP-ILUC to converge for various r/λ are shown in Table 7. The symbol '–' in the table indicates that convergence was not obtained in 1000 iterations or was terminated with an overflow condition. The value of r/λ can be fixed on 0.7 for our example.

7. Conclusions

In the first part of this paper, we have applied GMRES-DR to the analysis of the boundary value problem related to the diffraction wave field around a very large floating structure (VLFS). We have succeeded in reducing the total computing times by 1/2 as compared with using restarted GMRES. GMRES-DR has the parameter l, which is the desired number of harmonic Ritz vectors. It has been found that the parameter l of GMRES-DR can be fixed on about $l/m = 1/10$ regardless of incident wavelengths λ, where m is the maximum size of the subspace.

In the second part, we have applied OSP-ILUC to our example. With application of OSP-ILUC we have succeeded in reducing the total computing times by 1/2–1/5 as compared without application of a preconditioner. OSP has the parameter r, which is the minimum distance of far points. We have computed the spectrum of the preconditioned matrix AM^{-1} and we have shown that the spectrum of AM^{-1} clusters as r increases. Moreover, we have shown that the value of r/λ can be fixed on 0.7.

Appendix A. Compact Operators

In this appendix, we describe the bounded operators [14] of the near field interactions and of the far field interactions, which are split into by the operator splitting preconditioner (OSP) [7]. We assume that the wetted-surface S_H is smooth.

In the first place, we rewrite the integral Eq. (10) and we show that the coefficient matrix A of the system of linear Eq. (1) is non-Hermitian. We set $E(\varepsilon) = \{(x,\xi) \in S_H \times S_H : ||x-\xi||_2 > \varepsilon\}$ and $\chi_{E(\varepsilon)}(x,\xi)$ is the function which has the value of 1 on $E(\varepsilon)$ and has the value of 0 otherwise, where ε is a positive number. We define an integral operator T on $X = L^2(S_H)$ to be

$$(Tu)(x) = \lim_{\varepsilon\to 0}\int_{S_H} \chi_{E(\varepsilon)}(x,\xi)\left\{\frac{\partial G(x,\xi)}{\partial n_\xi}u(\xi) - \frac{\partial G_2(x,\xi)}{\partial n_\xi}u(x)\right\}\mathrm{d}\xi (x \in S_H), \tag{A.1}$$

then T is a compact operator [14] on X (see Ref. [2]), where $G(x,\xi)$ is the free-surface Green's function and $G_2(x,\xi)$ is the auxiliary Green's function [12]. Here, $L^2(S_H)$ is the Hilbert space [14] of all square integrable complex functions on S_H. Then the integral equation (10) is rewritten as

$$(4\pi I + T)\phi = 4\pi\phi_I. \tag{A.2}$$

We can see that T is not a self-adjoint operator [14] on X. Since the adjoint operator T^* of T is

$$(T^* v)(x) = \lim_{\varepsilon\to 0}\int_{S_H} \chi_{E(\varepsilon)}(x,\xi)\left\{\frac{\overline{\partial G(\xi,x)}}{\partial n_x}v(\xi) - \frac{\overline{\partial G_2(x,\xi)}}{\partial n_\xi}v(x)\right\}\mathrm{d}\xi (x \in S_H), \tag{A.3}$$

this implies that $T^* \neq T$. Therefore, it is found that the coefficient matrix A of the system of linear equations (10) which arises from the integral equation (A.2) is non-Hermitian.

In the second place, we define compact operators $T_{near}(r)$ and $T_{far}(r)$ on X and we show that it can be expected all eigenvalues of AM^{-1} which is transformed by the preconditioner M will cluster around 1. Let r be a positive real number. We set $F(\varepsilon, r) = \{(x,\xi) \in S_H \times S_H : \varepsilon < ||x-\xi||_2 \le r\}$ and we define an integral operator $T_{near}(r)$ on X to be

$$(T_{near}(r)u)(x) = \lim_{\varepsilon\to 0}\int_{S_H} \chi_{F(\varepsilon,r)}(x,\xi)\left\{\frac{\partial G(x,\xi)}{\partial n_\xi}u(\xi) - \frac{\partial G_2(x,\xi)}{\partial n_\xi}u(x)\right\}\mathrm{d}\xi. \tag{A.4}$$

Also, we define an integral operator $T_{far}(r)$ on X to be

$$(T_{far}(r)u)(x) = \int_{S_H} \chi_{E(r)}(x,\xi)\left\{\frac{\partial G(x,\xi)}{\partial n_\xi}u(\xi) - \frac{\partial G_2(x,\xi)}{\partial n_\xi}u(x)\right\}\mathrm{d}\xi. \tag{A.5}$$

Both $T_{near}(r)$ and $T_{far}(r)$ are compact and the bounded operator T has the following splitting form:

$$T = T_{near}(r) + T_{far}(r). \tag{A.6}$$

The preconditioner M by OSP is a matrix arising from the bounded operator $N(r) = 4\pi I + T_{near}(r)$. $N(r)$ is injective if r is chosen not to be too large, $N(r)$ is surjective because $T_{near}(r)$ is compact, so $N(r)^{-1}$ is bounded by the open mapping theorem [14]. The bounded operator transformed by $N(r)$ is

$$(4\pi I + T)N(r)^{-1} = I + T_{far}(r)N(r)^{-1}, \tag{A.7}$$

$T_{far}(r)N(r)^{-1}$ is compact because $T_{far}(r)$ is compact and $N(r)^{-1}$ is bounded, so the spectrum of $T_{far}(r)N(r)^{-1}$ has at most one limit point, namely 0. Therefore, it can be expected that all eigenvalues of AM^{-1} which arises from the left side of (A.7) will cluster around 1.

References

[1] Utsunomiya T, Watanabe E. Wave response analysis of hybrid-type VLFS by accelerated BEM. Proceedings of third int conf hydroelasticity in marine technology 2003 p. 297–303.

[2] Amini A, Harris J, Wilton DT. Coupled boundary and finite element methods for the solution of the dynamic fluid-structure interaction problem. New York: Springer; 1992.

[3] Saad Y, Schultz MH. GMRES: a generalized minimal residual algorithm for solving nonsymmetric linear systems. SIAM J Sci Stat Comput 1986; 7:856–69.

[4] Morgan RB. GMRES with deflated restarting. SIAM J Sci Comput 2002; 24:20–37.

[5] Saad Y. Numerical methods for large eigenvalue problem. New York: Halsted Press; 1992.

[6] Nachtigal NM, Reddy SC, Trefethen LN. How fast are nonsymmetric matrix iterations? SIAM J Matrix Anal Appl 1992;13:778–95.
[7] Chen K. An analysis of sparse approximate inverse preconditioners for boundary integral equations. SIAM J Matrix Anal Appl 2001;22:1058–78.
[8] Schneider S, Marburg S. Performance of iterative solvers for acoustic problems. Part II. Acceleration by ILU-type preconditioner. Eng Anal Bound Elem 2003;27:751–7.
[9] Li N, Saad Y, Chow E. Crout version of ILU for general sparse matrices. SIAM J Sci Comput 2003;25:716–28.
[10] Greengard L. The rapid evaluation of potential fields in particle systems. Massachusetts: MIT Press; 1988.
[11] Utsunomiya T, Watanabe E, Nishimura N. Fast multipole algorithm for wave diffraction/radiation problems and its application to VLFS in variable water depth and topography. Proceedings of 20th int conf on offshore mechanics & arctic engineering 2001 [OMAE01-5202].
[12] Teng B, Eatock Taylor R. New higher-order boundary element methods for wave diffraction/radiation. Appl Ocean Res 1995;17:71–7.
[13] Zhang SL. GPBi-CG: generalized product-type methods based on Bi-CG for solving nonsymmetric linear systems. SIAM J Sci Stat Comput 1997; 18:537–51.
[14] Rudin W. Functional analysis. 2nd ed. New York, NY: McGrow-Hill Book Company; 1991.